Received: 1 February 2022 | Revised: 21 April 2022 | Accepted: 21 April 2022

DOI: 10.33012/navi.526

ORIGINAL ARTICLE

Characterization and Performance Assessment of BeiDou-2 and BeiDou-3 Satellite Group Delays

Oliver Montenbruck[1] | **Peter Steigenberger**[1] | **Ningbo Wang**[2] | **André Hauschild**[1]

[1] Deutsches Zentrum für Luft- und Raumfahrt (DLR), German Space Operations Center (GSOC), 82234 Weßling, Germany

[2] Chinese Academy of Sciences (CAS), Aerospace Information Research Institute (AIR), No 9 Dengzhuang South Road, Beijing 100094, China

Correspondence
Oliver Montenbruck, DLR/GSOC, Münchener Str. 20, 82234 Weßling, Germany
Email: oliver.montenbruck@dlr.de

Abstract

Based on one year of data, a comprehensive assessment of broadcast group delays and differential code biases (DCBs) from network solutions is presented for all open BeiDou signals. Daily DCB estimates exhibit a precision of 0.1 ns, which also places a limit on long-term variations of the satellite group delays. On the other hand, the estimated DCBs show a notable dependence on the employed receivers, which causes inconsistencies at the few-nanosecond level between BeiDou-2 and BeiDou-3 satellites. Systematic satellite-specific offsets can likewise be identified in broadcast group delay values and clock offsets. These constitute the dominant contribution of the signal-in-space range error (SISRE) budget and are a limiting factor for single point positioning and timing. Use of the modernized B1C/B2a signals is therefore recommended instead of B1I/B3I. This offers a SISRE reduction from about 0.6 m to 0.45 m and also improves the consistency of precise clock and bias products derived from heterogeneous receiver networks.

Keywords

BeiDou, DCB, group delays, ISC, SISRE, TGD

1 | INTRODUCTION

Following GPS, GLONASS, and Galileo, the Chinese BeiDou-3 system (BDS-3) started to provide navigation services for worldwide users in late 2019. Other than the second-generation BeiDou-2 system (BDS-2), which is mainly composed of satellites in geostationary Earth orbits (GEOs) and inclined geosynchronous orbits (IGSOs), BDS-3 is also comprised of 24 medium Earth orbit (MEO) satellites in three orbital planes that provide a global coverage. As the youngest global navigation satellite system (GNSS), BDS-3 makes use of highly advanced signal modulations and offers open service signals on five different frequencies. Along with a favorable signal-in-space range error (Montenbruck et al., 2020), which matches or even exceeds that of GPS, BDS-3 recommends itself as a highly competitive navigation system for worldwide users.

Other than GPS and Galileo, which refer the satellite clock offset information in their broadcast navigation data to an ionosphere-free dual-frequency signal combination, BDS-2 and BDS-3 provide satellite clock offsets for the B3 frequency. Except for the uncommon case of a B3 single-frequency user, satellite group delays

will always need to be considered in both single-frequency and dual-frequency positioning using BDS-2 and BDS-3 code observations to relate the satellite clock offsets to the specific signals chosen by the BeiDou user. For this purpose, the navigation messages transmitted by the BeiDou satellites include both *timing group delays* (TGDs), which provide differential code biases (DCBs) of selected signals in the B1 and B2 bands relative to the B3 clock reference signal, as well as *inter-signal corrections* (ISCs) providing DCBs between specific pairs of signals in the same frequency bands.

Evidently, the quality of code-based positioning thus depends not only on the quality of satellite orbit and clock information, but also on the quality of the group delay data. This is particularly detrimental for timing applications, since access to BeiDou system time (BDT) through ionosphere-free dual-frequency observations depends directly on the availability and quality of the respective group delay parameters. Proper knowledge of group delays is also important for precise point positioning techniques to reduce convergence times and facilitate carrier-phase ambiguity fixing.

While numerous publications have already discussed the quality of broadcast TGDs and DCBs observed with public receiver networks for the BDS-2 constellation (Guo et al., 2015; Montenbruck et al., 2014; Wang et al., 2016; Zhang et al., 2020a), only an incomplete characterization is presently available for the third-generation system. This is partly related to limitations in the supported signal set and the range of pseudorandom noise (PRN) numbers supported by early BDS-3 receivers, but also the lacking support for broadcast ephemeris of the modernized civil navigation (CNAV) messages of BDS-3 in public data archives. Within the network of the International GNSS Service (IGS; Johnston et al., 2017), tracking the new BDS-3 signals has only been achieved as of early 2021, and CNAV-1/2/3 navigation messages with associated group delay parameters are only supported in the most recent version 4.0 of the Receiver Independent Exchange format (RINEX; Romero, 2021) released in late 2021.

Early DCB estimates for the BDS-3S in-orbit validation satellites were presented in Li et al. (2019) based on observations of the IGS network and the international GNSS Monitoring and Assessment System (iGMAS; Cai et al., 2016). However, these satellites do not form part of the operational BDS-3 system and differ from the final constellation in various aspects of their signal structure. Initial results on BeiDou-3 are reported in Wang et al. (2020) who analyzed differential code biases for the legacy B1 and B3 signals of BDS-2 and BDS-3 satellites derived from a global receiver network using one month of data from early 2019. They point out a receiver-type dependency for the mean offset between the satellite DCBs of the second-generation and third-generation satellites. Likewise, Zhang et al. (2020c) discussed TGDs for the legacy BDS-2 and BDS-3 signals on the B1 frequency relative to B3 for 6 months of data in 2019. The authors demonstrated that DCBs derived from observations of the IGS network provide better positioning performance than the broadcast TGD_1 values. However, given only partial constellation deployment and limited receiver capabilities in the study periods, only BDS-3 satellites with PRNs C19 to C37 were covered in both analyses.

The latter constraint applies as well for Zhu et al. (2020), who discussed the determination of differential code biases of the BDS-3 B1C, B2a, and B2b signals relative to the B3 signal from observations of iGMAS sensor stations. Using the BeiDou Global Ionospheric Delay Correction Model (BDGIM) broadcast ionosphere model for the correction of ionospheric path delays, a 1 to 2 ns accuracy was obtained for

weekly averages. While of interest from a methodological point of view, no routine bias product was provided as part of that work. Also, it remains unclear how the resulting biases compare with biases that have previously been determined as part of the BDGIM generation process within the BeiDou control segment as well as the TGDs transmitted in the BDS-3 navigation message.

Li et al. (2020) analyzed code and phase biases for the modernized BDS-3 signals on the B1 and B2a/B2b frequencies. The analysis was based on observations of the first eight BDS-3 satellites obtained from iGMAS sensor stations and shows almost identical data-pilot DCBs for B2a and B2b signals, as well as small (few ns) biases between signals in the adjacent frequency bands. For the data-pilot DCBs of the modernized B1 signal, a 1-ns scatter across the available set of satellites was observed. Given a focus on bias determination and characterization for precise point positioning applications, no comparison with broadcast group delays was performed by the authors of that work. BDS-3 DCBs of legacy and modernized signals were also discussed in Gu et al. (2020). However, the study was mostly conceptual in nature and compared the quality of DCBs determined from triple-frequency observations in an undifferenced (UD) processing with those derived from a traditional approach using pseudorange differences and global ionosphere maps (GIMs). However, a slightly better repeatability of daily DCB estimates was obtained with GIMs due to limitations in the BDS-3 orbit and clock product quality that affected the UD processing scheme.

Wang et al. (2019) compared broadcast TGDs of BDS-2, BDS-3S, and the first 18 BDS-3 satellites with DCB products derived from the Chinese Academy of Sciences (CAS) and the German Aerospace Center (DLR) from observations of the IGS multi-GNSS network. Their analysis revealed an inconsistency of roughly 4 ns between BDS-2 and BDS-3 satellites in the mean difference of the TGD_1 broadcast group delay and the network solutions of the B1-B3 DCBs. This offset was further investigated in Zhang et al. (2020b), who revealed a notable dependence on receiver type. Considering the three different receiver models used in the IGS network at the time of their study, the authors obtained mean differences $(TGD_1 - DCB_{B1\text{-}B3})_{BDS\text{-}3} - (TGD_1 - DCB_{B1\text{-}B3})_{BDS\text{-}2}$ of 1.7 ns, 3.3 ns, and 5.3 ns, respectively. Similar to Wang et al. (2019), the analysis was limited to a subset of the full BDS-3 constellation.

The issue of receiver-dependent effects in the determination of satellite group delays has earlier been addressed by the control segment for the BeiDou-2 system and resulted in a major update of BDS-2 broadcast TGD values in mid-2017. While TGDs prior to July 21, 2017, were based on measurements with narrow correlator reference receivers, they were replaced by TGDs measured with a wide-correlator receiver in this epoch. As discussed in Zhang et al. (2020a), TGD changes for individual satellites amounted in up to 4 ns or roughly 1.2 m and were found to provide better consistency with group delays inferred from geodetic receivers in the IGS monitoring network. Furthermore, single point positioning errors were clearly reduced when using the new TGD values.

An initial discussion of group delays for the complete BDS-3 constellation is provided in Li and Yuan (2021) based on 6 months of data from the IGS and iGMAS networks in 2020. However, a notably degraded consistency of different DCB products may still be noted for PRNs above C37 as compared to the lower PRN range due to the reduced number of supporting stations. Beyond the legacy signals, selected bias determination results were also presented for the modernized BDS-3 signals, but interpretation of the results is partly hampered by the use of non-standard signal designations and the incorporation of non-public signal components that are not accessible to common geodetic receivers.

With this background in mind, the present study provides a comprehensive characterization of broadcast group delays as well as publicly available differential code bias products derived from global receiver networks covering the entire year of 2021. The work makes use of broadcast group delays in legacy (D1/D2) and modernized (CNAV-1/2/3) navigation messages extracted from raw navigation data of roughly 35 globally distributed receivers and made available in the *BRD4* merged RINEX 4 navigation files (Montenbruck & Steigenberger, 2022). DCBs derived from the analysis of IGS monitoring stations are presently made available by CAS (Wang et al., 2016) and DLR (Montenbruck et al., 2014) through IGS data centers. The stability and consistency of individual group delays in these products are evaluated and the values are compared with the broadcast group delays.

The article starts with an overview of BDS-2 and BDS-3 signals with a focus on openly accessible signal components fully described in associated interface control documents (ICDs). Next, the basic observation model for differential code biases is introduced, which forms the basis for group delay determination with or without background ionosphere data (Section 3). Along with this, the impact of frequency-dependent antenna phase center offsets and patterns is discussed as a prerequisite for a consistent analysis of current and future DCB products. Section 4 addresses basic characteristics of BDS-2 and BDS-3 broadcast group delays received throughout the year 2021 and discusses the updates performed by the BeiDou control center in this period. A comparison and stability assessment of CAS and DLR DCB products is provided in Section 5 and complemented by an analysis of receiver dependencies of satellite group delay estimates (Section 6). The overall impact of these effects on the consistency of broadcast group delays and DCBs from monitoring networks is discussed in Section 7, which evaluates the overall signal-in-space range error for individual single-frequency signals and dual-frequency combinations. A summary and final conclusions are provided in Section 8.

2 | BEIDOU SIGNAL OVERVIEW

The BeiDou constellation (Lu & Yao, 2020) transmits a diverse set of signals on a total of five distinct frequencies (Figure 1). These include three legacy signals known as B1I, B2I, and B3I, which were introduced as part of the second-generation regional BeiDou system (BDS-2). For compatibility reasons, B1I and B3I signals continue to be transmitted by the satellites of the third-generation global system (BDS-3; Yang et al., 2019) as well as a small number of intermediate BDS-3S test satellites. The latter can be tracked by various types of receivers but are not considered part of the operational BeiDou constellation.

As part of the global BDS-3 system, modernized B1C, B2a, and B2b signals were introduced that share the center frequency of the GPS/Galileo L1/E1, L5/E5a, and E5b signals. B1C and B2a include both data and pilot components and offer improved tracking compared to B1I and B2I due to their advanced modulation and chipping rates. For B2b, only a data component is presently defined, but a second quadrature channel is transmitted on BDS-3 MEO and IGSO satellites that has already been tracked successfully by selected geodetic receivers despite the lack of a formal signal specification. Finally, it is mentioned that the B2a and B2b signals result from a common *asymmetric constant envelope binary offset carrier* (ACE-BOC) modulation covering the combined B2ab band (Lu et al., 2019; Yao et al., 2016). Similar to the Galileo E5ab AltBOC (alternative binary offset carrier) signal, various geodetic receivers already support a combined tracking of B2a and B2b as a single wideband signal with very low noise and multipath.

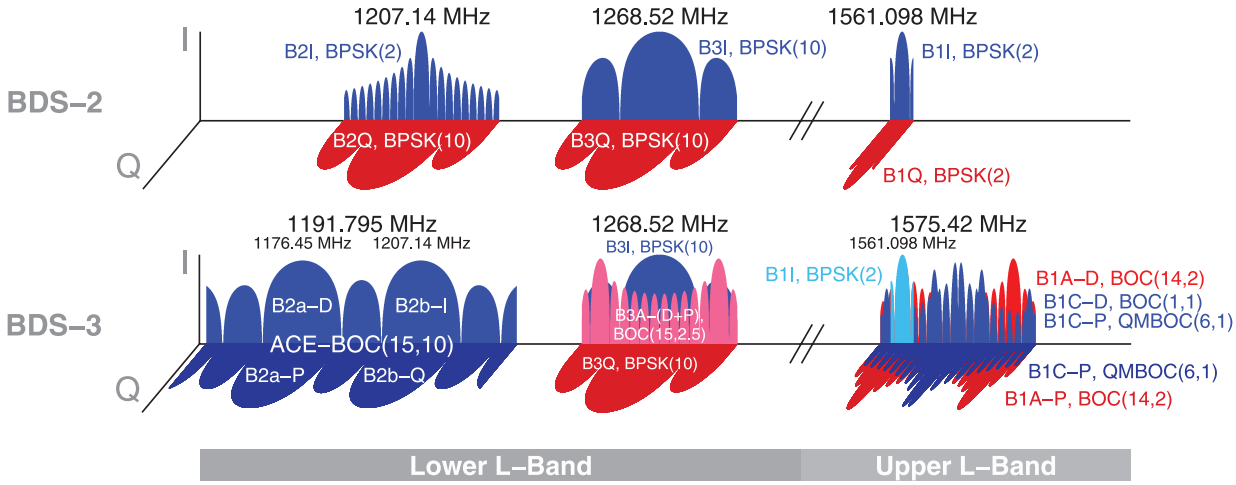

FIGURE 1 Schematic representation of BeiDou-2 and BDS-3 signal spectra in the lower and upper L-band; blue and red colors indicate open service and restricted signals, respectively. In-phase (I) and quadrature-phase (Q) components are shown on orthogonal planes. Next to its name, the modulation scheme is indicated for each signal (BPSK: binary phase shift keying; BOC: binary offset carrier; QMBOC: quadrature multiplexed binary offset carrier; ACE-BOC asymmetric constant envelope binary offset carrier). Numbers in brackets denote the chipping rates of the ranging codes and sub-carriers in multiples of 1.023 MHz.

TABLE 1
BeiDou Open Service Signals

Signal	Band	f_0 [MHz]	RINEX	Nav. Msg.	Satellites
B1C(d+p)	B1	1575.420	C1D/P/X	CNAV-1	BDS-3
B1I	B1-2	1561.098	C2I	D1/D2	BDS-2/3S/3
B3I	B3	1268.520	C6I	D1/D2	BDS-2/3S/3
B2I	B2b	1207.140	C7I	D1/D2	BDS-2
B2b-I/[Q]	B2b	1207.140	C7D/P/Z	CNAV-3	BDS-3
B2a(d+p)	B2a	1176.450	C5D/P/X	CNAV-2	BDS-3
[B2ab]	B2ab	1191.795	C8D/P/X	–	BDS-3

Note: Square brackets denote selected signals that are transmitted and can be tracked by various receivers but are not formally described as part of an official signal specification. Next to the center frequency f_0, the corresponding RINEX observation codes and the navigation messages transmitted on the respective signals are provided.

An overview of the various openly accessible signals broadcast by BeiDou satellites today is provided in Table 1. Details of the signal structure, modulation, and data content of each of these signals are provided in the respective ICDs (CSNO, 2016, 2017a, 2017b, 2018, 2019, 2020) as well as Betz (2016) and Lu et al. (2019).

Similar to modernized signals of other constellations, current geodetic receivers employ different strategies for the handling of data and pilot signal components in the new BDS-3 signals. With very limited exceptions, two categories of receivers may presently be distinguished. A first group of receivers, including models of Septentrio and Leica, makes exclusive use of the pilot component for the generation of pseudorange and phase measurements, while others (including Javad and Trimble) make joint use of the data and pilot component in the B1C and B2a signals. The respective observations are distinguished by a *P* (pilot-only) and *X* or *Z* attribute (data+pilot) in the corresponding RINEX identifiers. With the exception of the B2b signal, for which only a data component is officially defined, no

receivers offering data-only observations were available in the IGS network as of late 2021, thus limiting the analysis of differential code biases to pilot-only or combined pilot-data tracking.

Despite a common center frequency and modulation scheme, pilot and data channels of multiplexed signals are usually affected by different group delays. In a combined pilot+data tracking, an average group delay will be observed that depends on the weighting of pilot and data signals in the respective tracking loops. For the specific test receiver examined in Sleewaegen and Clemente (2018), biases for pilot+data tracking of the Galileo E1 signal were found to equal the arithmetic average of pilot-only and data-only tracking. Other than current GPS, Galileo, and QZSS signals, which employ equal power sharing for the data and pilot channels, a 1:3 power ratio is used in the BDS-3 B1C signal (CSNO, 2017a). As such, group delays for X observations are likely dominated by the pilot signal and can reasonably well be compared with the respective biases derived from pilot-only receivers. For the B2a signal, in contrast, equal power sharing is used which hampers a comparison of C5X and C5P code biases.

3 | PSEUDORANGE AND DCB OBSERVATION MODEL

Following Hauschild (2017), pseudorange observations in precise positioning and timing applications can be described by the generic model:

$$\begin{aligned} P = &|| \boldsymbol{r}^{\mathrm{sat}} - \boldsymbol{r}_{\mathrm{rcv}} || + \boldsymbol{e}^T \boldsymbol{r}^{\mathrm{sat}}_{\mathrm{pco}} - \boldsymbol{e}^T \boldsymbol{r}_{\mathrm{pco,rcv}} + \xi^{\mathrm{sat}} - \xi_{\mathrm{rcv}} \\ &+ cdt^{\mathrm{sat}} - cdt_{\mathrm{rcv}} + T + I + b^{\mathrm{sat}} + b_{\mathrm{rcv}} \end{aligned} \tag{1}$$

where $\boldsymbol{r}^{\mathrm{sat}}$ and $\boldsymbol{r}_{\mathrm{rcv}}$ denote the antenna reference point positions of the satellite and receiver, $\boldsymbol{e}$ is the line-of-sight unit vector from the receiver to the satellite, $\boldsymbol{r}_{\mathrm{pco}}$ denotes the respective code phase center offsets (PCOs), and ξ represents any additional direction-dependent group delay variations (GDVs). Furthermore, cdt^{sat} and cdt_{rcv} are the satellite and receiver clock offsets, and T and I denote the tropospheric and ionospheric path delays. Finally, signal-specific pseudorange biases are described by the additional terms b^{sat} and b_{rcv}.

Here, it is assumed for practical reasons that the total group delay can be fully separated into distinct satellite and receiver contributions that add up in the pseudorange model. It should be noted, however, that satellite-specific chip shape distortions will result in ranging biases that depend on the correlator architecture and spacing. These may cause inconsistencies of up to several nanoseconds between satellite DCBs derived with different receivers (Hauschild & Montenbruck, 2016; He et al., 2020) and inhibit a fully consistent partitioning of the total group delay into satellite and receiver contributions.

Based on the above model, the differential code biases $\mathrm{DCB}(\mathrm{s}_1,\mathrm{s}_2) = b_{\mathrm{s}_1} - b_{\mathrm{s}_2}$ for two signals s_1 and s_2 can be related to the difference of the respective pseudorange observations after accounting for the difference in ionospheric path delays and, if needed, correcting for signal-specific differences in phase center offsets and group delay patterns:

$$\begin{aligned} &\mathrm{DCB}(\mathrm{s}_1,\mathrm{s}_2)^{\mathrm{sat}} + \mathrm{DCB}(\mathrm{s}_1,\mathrm{s}_2)_{\mathrm{rcv}} \\ &= (P_{\mathrm{s}_1} - P_{\mathrm{s}_2}) - (I_{\mathrm{s}_1} - I_{\mathrm{s}_2}) \\ &\quad - \boldsymbol{e}^T (\boldsymbol{r}^{\mathrm{sat}}_{\mathrm{pco},\mathrm{s}_1} - \boldsymbol{r}^{\mathrm{sat}}_{\mathrm{pco},\mathrm{s}_2}) + \boldsymbol{e}^T (\boldsymbol{r}_{\mathrm{pco},\mathrm{s}_1,\mathrm{rcv}} - \boldsymbol{r}_{\mathrm{pco},\mathrm{s}_2,\mathrm{rcv}}) \\ &\quad - (\xi^{\mathrm{sat},\mathrm{s}_1} - \xi^{\mathrm{sat},\mathrm{s}_2}) + (\xi_{\mathrm{rcv},\mathrm{s}_1} - \xi_{\mathrm{rcv},\mathrm{s}_2}) \end{aligned} \tag{2}$$

Depending on a trade-off of timeliness, processing effort, and dependence on external data products, ionospheric path delays may either be taken from pre-computed global ionosphere maps (Montenbruck et al., 2014; Zhu et al., 2020) or determined together with differential code biases in a combined analysis (Wang et al., 2016). To reduce the impact of pseudorange measurement noise and multipath, observations are typically averaged over daily observation intervals, unless known switches in the transmitter configuration require a corresponding choice of tailored data arcs (Esenbuga et al., 2020). Furthermore, the raw pseudorange observations may be substituted by carrier-smoothed pseudoranges (Hwang et al., 1999) or code-aligned phase observations (Wilson & Mannucci, 1994).

The need for consideration of signal-specific PCOs in the estimation of DCB products is driven by the observation model used for positioning and may differ among applications. In the case of broadcast ephemerides, a common transmit antenna phase center is implied for all signals and frequencies of a given satellite, and the broadcast orbit parameters directly provide the position of this phase center in space. Likewise, all broadcast group delays apply for a common-phase-center observation model without consideration of direction-dependent group delay variations.

For precise point positioning (PPP) applications, in contrast, phase center offsets are commonly taken from the IGS antenna model (Rebischung & Schmid, 2016). This has traditionally been based on observed phase centers for the ionosphere-free combination of dual-frequency observations and jointly utilizes those phase centers for the modeling of individual frequencies. In contrast, frequency-specific PCOs for BDS-2 and BDS-3 satellites have been published by the Chinese Satellite Navigation Office (CSNO) after the build-up of the global constellation (CSNO-TARC, 2022).

Based on these data, block-specific and frequency-specific phase center offsets for BDS-2 and BDS-3 satellites were included in the IGS antenna model starting with igs14_2069.atx. Direction-dependent group delay variations have been identified in various studies for the BDS-2 satellites (Lou et al., 2017; Wanninger & Beer, 2015), whereas BDS-3 satellites were shown to be essentially free of such variations (Beer et al., 2021; Hong et al., 2020). However, no common standard for the application of satellite GDVs exists and their consideration is presently left to the discretion of individual analysis centers and users.

Despite the availability of frequency-specific PCO information, all IGS DCB products so far are based on a common-phase-center model and transition to PCO-dependent DCB modeling is only foreseen for mid-2022 along with the introduction of a new IGS antenna model (Banville, 2021). As such, broadcast group delays can directly be compared with IGS DCB products in the present study, but the use of IGS (and broadcast) DCB inhibits the direct use of this data in PPP models. In the absence of GDV contributions, satellite DCBs compatible with the full observation model (marked by an asterisk) can be obtained from DCBs of a common-phase-center model by accounting for the approximate difference of the PCO z-coordinates for the two signals in the spacecraft body frame:

$$\mathrm{DCB}^{*}(s_1, s_2)^{\mathrm{sat}} = \mathrm{DCB}(s_1, s_2)^{\mathrm{sat}} - (z^{\mathrm{sat}}_{\mathrm{pco},s_1} - z^{\mathrm{sat}}_{\mathrm{pco},s_2}) \tag{3}$$

This approximation is based on the averaging of Equation (2) over all the boresight angles of the nadir-oriented transmit antenna is generally good to better than a few centimeters.

4 | BEIDOU BROADCAST GROUP DELAYS

As part of the D1/D2 legacy navigation messages, all BDS satellites transmit a TGD_1 timing group delay, which reflects the bias of the B1I signal relative to the B3I reference (i.e., the C2I-C6I DCB [Table 2]). For BDS-2 satellites, an additional TGD_2 parameter corresponding to the C7I-C6I DCB is also provided in these messages. In D1/D2 messages of BDS-3 satellites, the TGD_2 field is populated with a copy of the TGD_1 value but has no practical meaning since no B2I signal is transmitted by those satellites.

Group delay parameters for the pilot component of the new B1C and B2a signals relative to B3I are jointly provided in the CNAV-1 and CNAV-2 messages. Furthermore, these messages also provide an inter-signal correction (ISC) that describes the differential code bias between the data and pilot channel of the respective signal. Finally, the CNAV-3 message provides a complementary group delay parameter for users of the B2b in-phase signal.

An overview of broadcast group delays transmitted by the various BeiDou satellites is given in Figure 2, which provides the annual means of the transmitted TGD/ISC values for each satellite. Colors from blue to red refer to individual spacecraft in the order of ascending space vehicle number [SVN]. The five columns within each sub-figure refer to BDS-2 satellites, BeiDou-3S in-orbit-validation satellites, BDS-3 GEOs+IGSOs, as well as BDS-3 MEO satellites built by CAST and SECM, respectively. Mean group delays over all satellites are indicated by horizontal lines. Complementary to the actual broadcast group delays, the figure also shows the differential code bias between the adjacent frequencies of the B1I and B1C signals as computed from the difference of the TGD_{B1Cp} and TGD_1 values. Despite the close proximity and the joint generation of these signals in a common wideband modulation scheme (Lu et al., 2019), the respective biases show a scatter of roughly ±4 ns across the various satellites of the BDS-3 constellation. For comparison, TGD_{B2bI}-TGD_{B2ap} group delay differences between the B2a and B2b sidebands of the B2ab ACE-BOC signal show a two-times smaller scatter despite a two-times larger frequency separation.

Overall, the group delays are most pronounced between signals in the upper (B1) and lower (B3, B2) L-Band, where values in the range of ±40 ns are encountered. Interestingly, a much larger scatter of TGD_1 and TGD_{B1Cp} values can be observed for BDS-3 satellites built by the China Academy of Space Technology (CAST) compared to those built by the Shanghai Engineering Center for Microsatellites (SECM) of the China Academy of Science (CAS). Inter-frequency biases between signals of the B3 and B2 band are typically confined to a range of about −10±10 ns, except for

TABLE 2
BeiDou Broadcast Group Delays

Navigation Message	Signal	Group Delay Parameter	RINEX Equivalent
D1/D2	B1I, B2I, B3I	TGD_1	C2I-C6I
		TGD_2	C7I-C6I
CNAV-1	B1C	TGD_{B1Cp}	C1P-C6I
		TGD_{B2ap}	C5P-C6I
		ISC_{B1cd}	C1D-C1P
CNAV-2	B2a	TGD_{B1Cp}	C1P-C6I
		TGD_{B2ap}	C5P-C6I
		ISC_{B2ad}	C5D-C5P
CNAV-3	B2b-I	TGD_{B2bI}	C7D-C6I

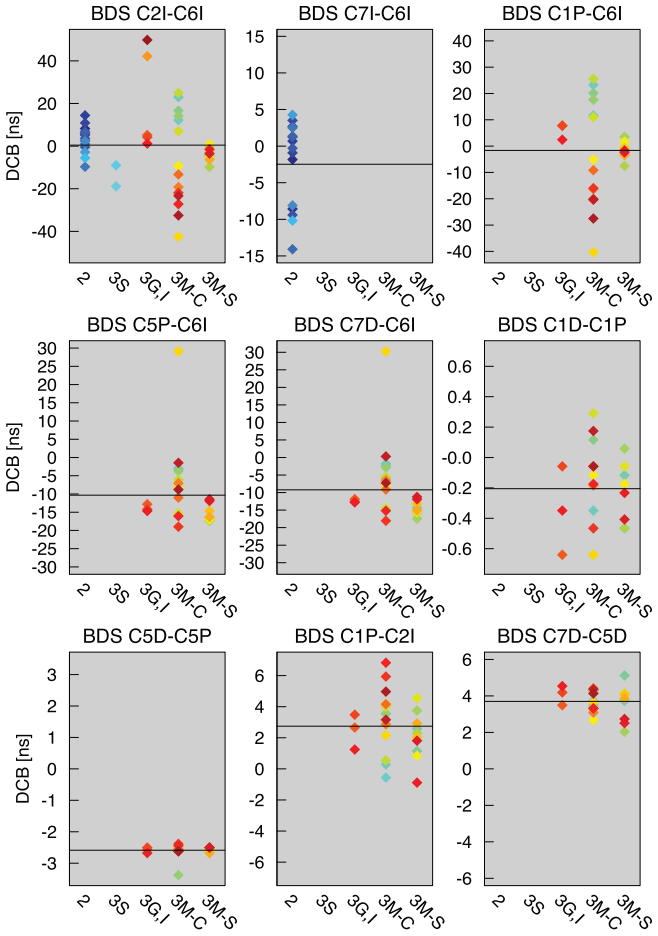

FIGURE 2 Mean values of broadcast DCBs provided in the BeiDou navigation messages over the year 2021

a single satellite (SVN C214 / PRN C33) which exhibits TGD_{B2ad} and TGD_{B2bI} values of about 30 ns. Intra-frequency biases between pilot and data components of the B1C and B2a signal, in contrast, show a very small scatter of well below 1 ns across the BDS-3 constellation.

Non-negligible mean values may be observed for various broadcast group delays, particularly for the TGD_{B2ap}, the TGD_{B2bI}, and the ISC_{B2ad}. Obviously, the broadcast group delay parameters of the BeiDou satellites determined by the control segment are not constrained by zero-constellation-mean conditions as used for IGS DCB products and the broadcast group delays of Galileo. On the other hand, the BeiDou signal specifications provide no information, on whether TGDs and ISCs are aligned to a calibrated golden receiver as done in GPS (Wilson & Mannucci, 1994; Yinger et al., 1999) or a reference satellite with pre-calibrated biases. However, the latter option is strongly suggested by the fact that TGD_1 and TGD_2 values transmitted by the first BDS-2 GEO satellite (SVN C003, PRN C01) until the end of March 2020 match the set of values identified as factory calibration data in Xing (2011). Following March 2020, SVN C018 (PRN C03) was apparently selected as a new pivot satellite by the BDS control segment, since it was the only BDS-2 satellite that transmitted constant TGD_1 and TGD_2 values thereafter, except for a temporary reconfiguration with TGD_1/TGD_2 switches of most BDS-2 satellites on September 2/3, 2021.

Concerning the modernized signals transmitted by the third-generation BeiDou satellites, it may be noted that constant values of all broadcast group delays are

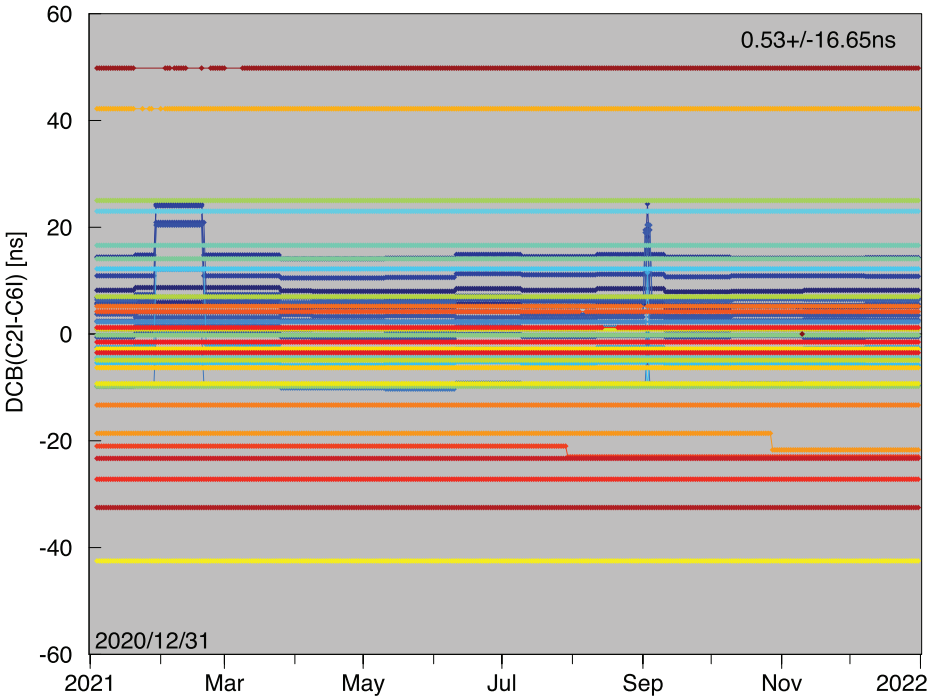

FIGURE 3 Temporal evolution of TGD_1 values transmitted in 2021 by BDS-2 and BDS-3 satellites (colors from blue to red refer to individual spacecraft in the order of ascending SVN)

transmitted in the CNAV-1/2/3 message of SVN C201 (PRN C19), while changes on individual TGDs or ISCs may be noted for all other satellites. This suggests that factory calibrations for the first BDS-3 MEO satellite are actually used as a reference for the broadcast group delays of the new B1C, B2a, and B2b signals.

Updates of the BDS-2 group delay parameters with changes at the sub-ns level were performed by the ground segment at intervals down to one month, but did not follow a strict schedule. In addition, two cases of anomalous broadcast group delays may be noted from January 28 to February 21 and September 2 to September 3. Here, TGD_1/TGD_2 changes at the level of 10 to 15 ns with respect to the normal values were encountered for multiple BDS-2 satellites (Figure 3). Since similar variations are obvious in IGS DCB products, reconfigurations of the satellite transmitter or navigation payload chains appear to be the most plausible explanation for the observed changes.

On BDS-3 satellites, only occasional changes of the broadcast TGDs could be noted on selected satellites. These were, likewise, reflected in IGS DCB estimates and can thus be attributed to spacecraft configuration changes. On September 18, 2021, a group delay change on Satellite C218 (C36) was observed in IGS monitoring. However, this change was only considered by a broadcast TGD update on October 28.

5 | IGS DCB PRODUCTS

Within the IGS, multi-GNSS differential code bias products are presently generated by two analysis centers and publicly made available through IGS data centers[1]. While CAS DCBs are estimated jointly with station-wise ionosphere

[1] https://cddis.nasa.gov/archive/gnss/products/bias/ and ftp://igs.ign.fr/pub/igs/products/mgex/dcb/

TABLE 3
Number of Stations Contributing to CAS and DLR DCB Products Near the Beginning and Ending of 2021

Signal	CAS		DLR	
	Begin	End	Begin	End
C2I	190	205	110	120
C6I	140	180	95	110
C7I	190	205	110	120
C1P	40	90	30	50
C1X	25	50	25	35
C5P	40	90	30	50
C5X	30	90	30	35
C7D			10	60
C7Z	20	35	20	20
C8X	20	35	15	15

parameters and provided on a daily basis (Wang et al., 2016) as a rapid product with a 2–3 day latency, the DCB solutions of DLR are based on external GIMs (Montenbruck et al., 2014) and made available in 3-month batches at the end of each quarter.

Both products are based on observations of the IGS multi-GNSS network but differ in the total number and distribution of stations. As shown in Table 3, the number of stations contributing BeiDou observations has continuously increased over the 1-year data period and includes about 140 to 200 stations tracking legacy B1I, B2I, and B3I signals. For the DLR product, a maximum of 120 stations was considered. Concerning the modernized B1C and B2a signals of BDS-3 satellites, two groups of receivers tracking either the combined data+pilot signal (X or Z) or the pilot-only component (P) may be distinguished.

In the case of the B2b signal, the publicly defined data component (C7D) is tracked by most stations, while combined pilot+data tracking (C7Z) was limited to just a single receiver type. Altogether, observations for the B1C and B2a signals were provided by about 70 to 180 receivers over the course of 2021. On the other hand, a notably lower number of stations support tracking the B2b signal or the combined B2ab ACE-BOC signal, which obviously limits the quality of the respective biases.

The stability of individual biases in the CAS and DLR DCB products is illustrated in Figure 4, which shows the distribution of standard deviations of individual DCBs across the BDS-2 and BDS-3 satellites. It is based on long-term statistics covering the full year of 2021 except for two periods from January 28 to February 21 and from September 1 through September 4. These periods included bias changes on multiple satellites that were attributed to ground or space system reconfigurations and have therefore been excluded from the stability analysis. For consistency, all DCBs were formed with respect to the B3I (RINEX C6I) signal, which is transmitted by all BDS-2 and BDS-3 satellites and also serves as reference for the broadcast group delays.

In the absence of calibrated reference receivers or satellites, the generation of daily DCBs by CAS and DLR makes use of a zero-mean condition across all contributing satellites to separate the total group delay into distinct satellite and receiver biases. Compared to broadcast TGDs, a systematic offset in these DCB products shows up that is common to all satellites in the constellation and will finally reflect

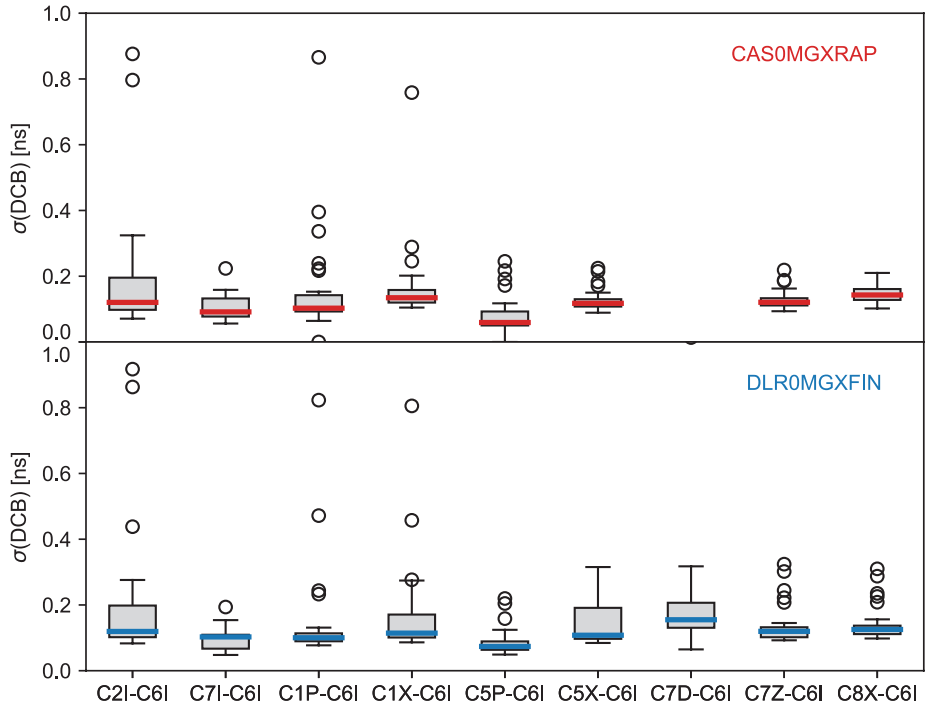

FIGURE 4 Box-whisker plots showing the median (colored lines), inter-quartile range (IQR; shaded boxes), and 1.5·IQR whiskers of standard deviations of individual satellite DCBs in the CAS and DLR products for the BDS-2 and BDS-3 constellation; outliers exceeding the 1.5·IQR limits are marked by open circles.

itself in a corresponding offset of the receiver clock estimate when using the different group delay values for navigation.

While positioning users may potentially benefit from a better compatibility of IGS DCBs with their receivers when using these DCBs instead of broadcast TGDs (Zhang et al., 2020a), the zero-mean alignment of IGS DCBs must be carefully considered in timing applications and hampers direct access to BeiDou system time. As illustrated in Figure 2, mean values of broadcast group delays across the constellation range from near zero values for the B1C data+pilot difference to values of about –10 ns for the TGDs of B2a and B2b group delays with respect to the B3I signal. Depending on the specific signal choice, notable inconsistencies may thus arise when switching between broadcast TGDs and IGS DCBs in the calibration of timing receivers (Li et al., 2021a).

Overall, both IGS DCB products achieved a median standard deviation of 0.08 to 0.15 ns, or, equivalently, 3 to 5 cm. These values provide an aggregate measure of the repeatability of daily bias estimates in the two products and the actual variability of the various satellite group delays. Individual outliers in the box-whisker plots can be attributed to occasional step changes with ns-level amplitudes in the biases of a small set of satellites. Except for such changes, which are likely related to onboard equipment changes or reconfigurations, the DCBs exhibit a favorable stability, which also justifies the strategy of rare broadcast ephemeris updates by the BeiDou control center.

DCBs in the two products exhibit a fairly similar stability. Furthermore, the stability of individual DCBs shows no obvious relation to the frequency separation of the contributing signals. This confirms that DCB estimation with pre-computed GIMs and code-only processing (as used in the DLR product) is, indeed, a viable and competitive approach for satellite group delay determination from a global

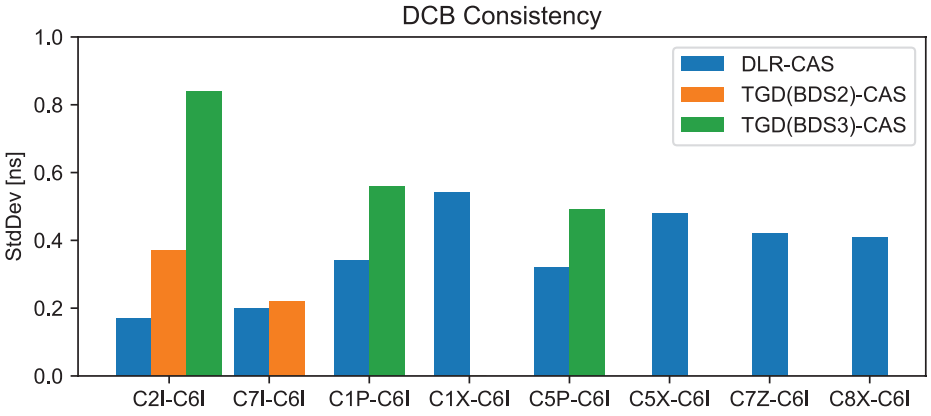

FIGURE 5 Standard deviation of DCB differences between DLR and CAS products, as well as broadcast TGDs and CAS DCBs

station network. Considering DCBs for individual signal pairs, the range of standard deviations (as shown by the size of the IQR boxes in Figure 4) is generally smaller for biases involving the modernized signals as compared to the C2I-C6I DCB for the legacy BDS-2 and BDS-3 signals. Within the DLR product, a larger spread of DCB standard deviations for data+pilot tracking of the B1C and B2a signal may be noted compared to DCBs for pilot-only tracking. This is mostly attributed to the smaller number of respective receivers in the network used for the DLR product.

While both the CAS and DLR DCB estimates exhibit a very favorable stability at the 0.1-ns level for each individual satellite, obvious satellite-specific offsets may be noted when differencing DCBs from the two products. Except for DCBs of legacy signals, which are tracked by the majority of receivers in the employed networks, DCB differences with a standard deviation of about 0.4 ns show up in the DLR-CAS comparison (Figure 5). Even though differences in the handling of ionospheric path delays in the DLR and CAS products will likely cause inconsistencies between the two products, the magnitude of these inconsistencies shows no relation to the frequency separation of signals in the individual DCBs.

Furthermore, differences in ionospheric path delay modeling would mostly cause random DCB differences, but are not expected to induce systematic satellite-specific effects in a global constellation. Therefore, the DCB differences can best be understood as the result of correlator-dependent offsets in the pseudorange observations of the contributing stations (Hauschild & Montenbruck, 2016). These show up most prominently when comparing DCBs from small networks with different shares of specific receiver types and thus affect DCBs for modernized signals more prominently than those of legacy signals in the current network configuration.

Similar issues are also evident when comparing broadcast group delays with DCBs from geodetic monitoring networks. As shown in Figure 5, TGDs for both legacy and modernized signals exhibited differences with a standard deviation of 0.4 ns to 0.9 ns relative to the CAS DCB products. These values notably exceed the internal precision of TGDs and DCBs and clearly reflect satellite-specific offsets between both types of bias products. By way of example, this is illustrated in Figure 6 for the TGD_1 (i.e., C2I-C6I group delay), which shows the most prominent offsets among all signals transmitted by the global BDS-3 system. A temporary step for Satellite C218 (C36; *gold*) in October 2021 reflects an onboard change that was immediately sensed by the CAS monitoring but only reflected in a TGD update with a one-month delay.

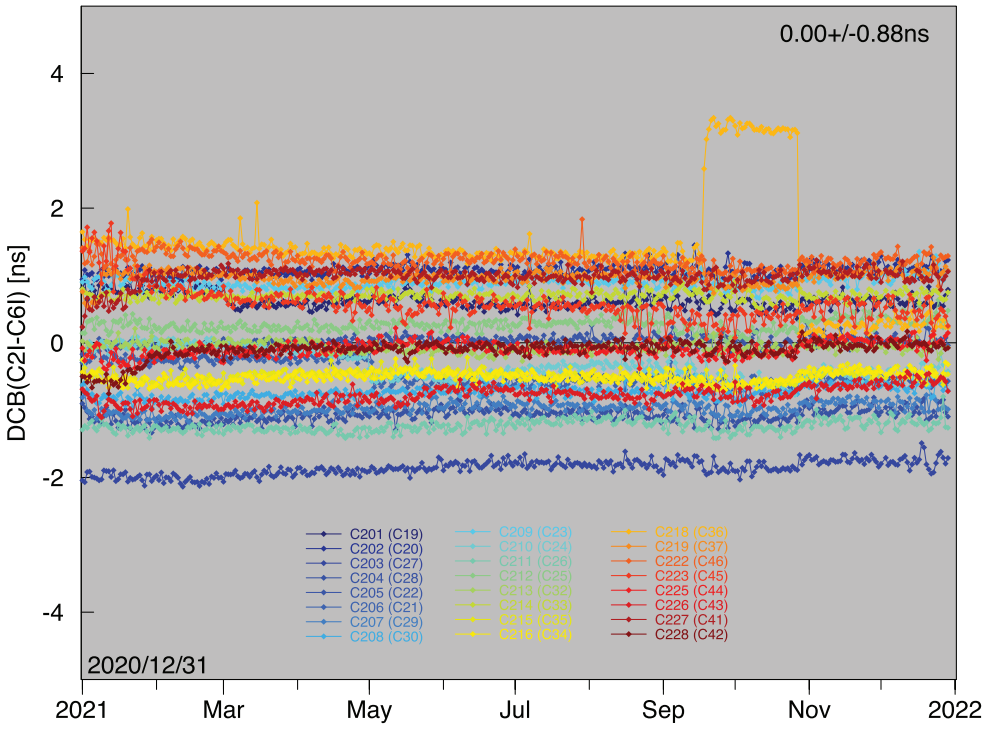

FIGURE 6 Differences of broadcast TGD_1 and CAS C2I-C6I DCBs for BDS-3 MEO satellites; colors from blue to red denote individual satellites in ascending SVN order.

6 | RECEIVER DEPENDENCY OF SATELLITE GROUP DELAYS

To further assess the satellite-specific inconsistencies in BeiDou TGDs and DCB products as well as their dependence on the employed receivers, we considered four selected subsets of the IGS network. Each of these supported the tracking of legacy and modernized BeiDou signals and is composed of stations with receivers of a single manufacturer based on a common architecture (Table 4). For each of the four networks, dedicated satellite DCBs were derived for a 16-day period (December 16 through December 31, 2021) using the same GIM-based approach as for the DLR0MGXFIN product (Montenbruck et al., 2014). Despite a reduced number of stations, individual DCB estimates obtained in these test cases exhibited a similar precision of about 0.1 to 0.2 ns (median standard deviation) as in the full network due to the shorter data arc.

For the comparison of type-specific receiver networks, we focused on the analysis of the C2I-C6I (TGD_1), C1P-C6I (TGD_{B1Cp}), and C1P-C5P ($TGD_{B1Cp} - TGD_{B2ap}$)

TABLE 4
Receiver-Type-Specific Subsets of IGS Network for BeiDou DCB Analysis

Set	Receivers		Number
1	Javad	TRE_3	30
2	Leica	GR10/25/30/50	15
3	Septentrio	AsterRx-4, PolaRx-4TR/-5/-5TR	30
4	Trimble	NetR9, Alloy	20–45

Note: The number of contributing stations may differ for legacy and modernized signals.

biases. Out of these, the first two DCBs directly represented the timing group delays of the legacy and modernized B1 signals relative to the B3I reference. Comparison of receiver-specific solutions for these DCBs and the associated TGD-DCB differences (Figures 7 and 8) showed that group delays for the legacy B1I signal exhibit the most significant impact of different receiver architectures, which seriously limits the applicability of TGD and DCB products in positioning with legacy BeiDou signals. A notably reduced receiver-dependence was observed for the B1C group delays relative to B3I and the B1C group delay relative to the B2a signal, which showed up in a smaller scatter of TGD-DCB values with a better consistency of the receiver-specific solutions.

With a total of almost 8 ns, the largest spread of $TGD_1 - DCB_{C2I\text{-}C6I}$ differences across the BeiDou constellation occurred for the network of Septentrio receivers, which was selected as a reference for the scatter plots in Figure 7. TGD-DCB differences for other receivers range from roughly one-third to two-thirds of this value and were smallest for the Javad receiver network. The data also illustrated a systematic offset in the TGD-DCB difference between BDS-2 and BDS-3 satellites that was first noted in Wang et al. (2019) and amounted to 5.2 ns, 1.6 ns, 3.0 ns, and 3.8 ns for receiver groups 1–4. These values were in good accord with previous results for Javad, Trimble, and Septentrio receivers presented in Zhang et al. (2020b) for a partial BDS-3 constellation including only satellites up to PRN C37. The inconsistencies of BDS-2 and BDS-3 biases can best be attributed to systematic differences in the chip shapes of the B1I signal. This signal is generated in a quadrature phase shift key (QPSK) modulation with only two signal components at the 1561.098-MHz center frequency in BDS-2 satellites, whereas a more sophisticated constant envelope multiplexing via intermodulation construction (CEMIC) scheme is used in BDS-3 satellites to jointly generate B1I along with the open B1C signal and the restricted B1A signal at 1575.42 MHz (Yao et al., 2017).

Evidently, this wideband modulation requires different signal generation hardware and resulted in different chip shapes for the B1I component than the narrowband modulation used on BDS-2. Depending on the front-end and correlator design, different receivers can sense different locations of the chip transition and thus group delays when tracking the B1I signals of different satellites. It must be emphasized, though, that these inconsistencies do not reflect specific strengths or weaknesses of individual receiver types, but are rather an inherent consequence

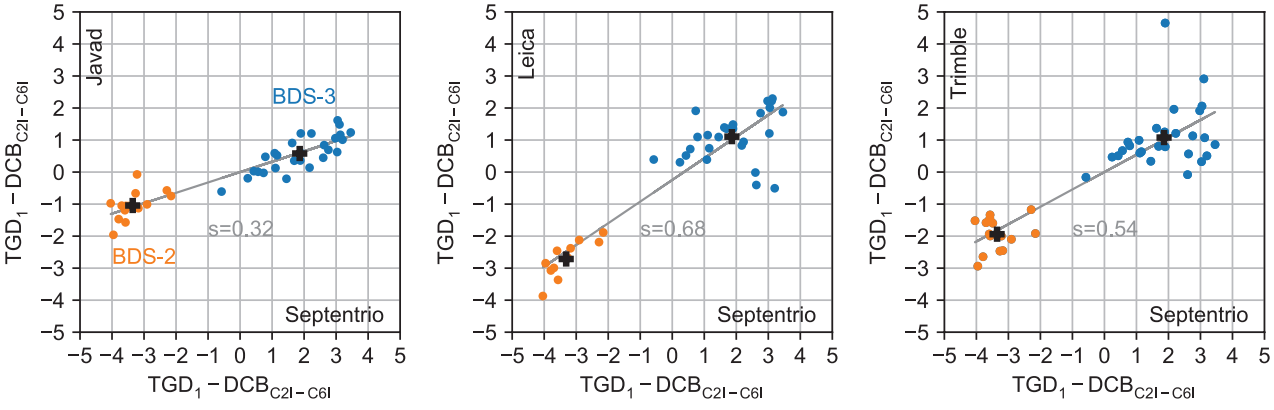

FIGURE 7 Scatter plot of $TGD_1 - DCB_{C2I\text{-}C6I}$ differences illustrating the receiver type dependence of B1I-B3I group delays (bold black plus signs indicate the mean value of the TGD-DCB difference for BDS-2 and BDS-3 satellites after zero-mean alignment of the constellation-wide differences; *s* denotes the slope of a trendline relating data for each receiver pair)

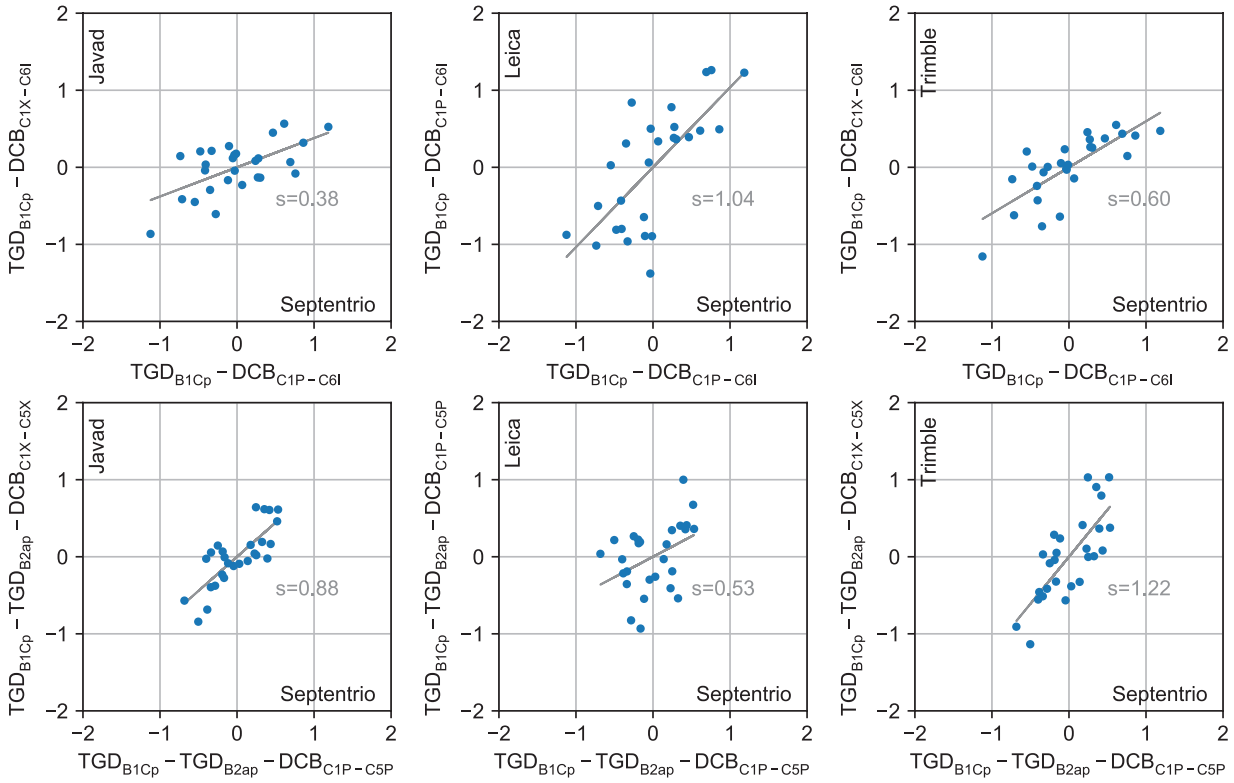

FIGURE 8 Scatter plot of $TGD_{B1Cp} - DCB_{C1P\text{-}C6I}$ and $TGD_{B1Cp} - TGD_{B2ap} - DCB_{C1P\text{-}C5P}$ differences illustrating the receiver type dependence of B1C-B3I and B1C-B2a group delays (in the case of Trimble and Javad receivers, pilot-only DCBs were substituted by DCBs from pilot+data tracking; *s* denotes the slope of a trendline relating data for each receiver pair)

of the limited consistency of the transmitted satellite signals across the BeiDou constellation. Likewise, the magnitude of the overall scatter of TGD-DCB differences in Figure 7 does not constitute a quality criterion per se, but rather represents the consistency of individual receiver types with the specific instruments for TGD determination in the BeiDou control segment.

Corresponding plots for the B1C-B3I and B1C-B2a group delays are shown in Figure 8, where, once again, an obvious correlation of the satellite-specific TGD-DCB differences among the various receivers may be noted. Different slopes of the individual trendlines illustrate a varying consistency of DCBs and TGDs across signals and receivers. Compared to the B1I-B3I group delay, individual slopes in the scatter plots are generally closer to unity, which suggests a better agreement of DCB estimates among different receivers. Irrespective of the agreement with broadcast TGD values, this fact ensures a better consistency of DCB estimates in heterogeneous networks and would also benefit the consistency of satellite clock estimates in BDS-3 precise orbit determination and time synchronization (Li et al., 2021b) from globally distributed monitoring stations.

Overall, the scatter of TGD-DCB differences is confined to typically less than ±1 ns and is thus at least two-times smaller than for the B1I-B3I group delays of the BDS-3 satellites. TGD–DCB differences for both B1P-B3I and B1P-B5P exhibit standard deviations of about 0.4 to 0.6 ns for the various receivers, which illustrates that both signals exhibit a similar quality in terms of chip shape consistency among all BDS-3 satellites. Use of these signals is therefore clearly preferable to B1I, if good positioning and timing accuracy is desired irrespective of the employed receiver type.

Even though a careful choice of signals may help to minimize the impact of receiver-dependencies in the determination and application of satellite group delays, it is unable to fully account for the coupling of receiver and satellite biases caused by GNSS signal distortions. As a remedy, the estimation of receiver-group-specific satellite group delays was proposed (Hauschild & Montenbruck, 2016) and is also foreseen in the definition of the bias SINEX exchange format (Schaer, 2016). Alternatively, a partitioning of the total group delays into a satellite contribution, a receiver contribution, and a complementary receiver-specific satellite contribution may be considered as proposed by Gong et al. (2018). However, both approaches have not yet found widespread attention and are presently not considered in the generation of IGS bias products. Likewise, they would not be practical for real-time users relying on broadcast group delays for single point positioning.

7 | POSITIONING AND TIMING

Stochastic and systematic errors in broadcast TGD and ISC values directly affect the quality of single point positioning (SPP) and timing solutions. To quantify this impact, we analyzed the signal-in-space ranging errors (SISRE) of BeiDou broadcast ephemerides considering different sets of user signals. The SISRE provides a location- and time-independent measure for the statistical contribution of broadcast orbit, clock, and group delay errors to the modeled pseudorange (Langley et al., 2017; Montenbruck et al., 2018). This pseudorange error can then be translated to the position and time domain by multiplication with the respective dilution-of-precision (DOP) factor for a given distribution of tracked satellites.

Using precise orbit, clock, and DCB products as a reference, the SISRE contribution of TGD/ISC errors may be assessed for individual sets of single- or dual-frequency user signals. Other than the direct comparison of broadcast group delays with network-based DCB solutions, the SISRE analysis also allowed us to identify correlations between group delay errors and errors in broadcast clocks. While the exact nature of these correlations cannot be identified without further insight into the process of broadcast ephemeris generation in the BeiDou control center, these correlations are important for a proper understanding of the individual SISRE error budgets and their knowledge enables an optimal signal choice in navigation and timing applications.

For our analysis, we made use of the GFZ0MGXRAP rapid orbit and clock solutions provided by Deutsches GeoForschungsZentrum Potsdam as part of the IGS multi-GNSS pilot project (Deng et al., 2017; Montenbruck et al., 2017) and complemented these with differential code biases of CAS (Wang et al., 2016). These reference clocks and DCBs are both based on observations of the IGS multi-GNSS network and can be considered as representative for an average geodetic-grade user receiver with multi-frequency tracking capability.

Broadcast and precise ephemerides refer to distinct antenna reference points and clock reference signals which must be considered in the comparison (Montenbruck et al., 2018). While broadcast orbit and clocks are referred to the B3 phase center as provided by CSNO (CSNO-TARC, 2022) and the B3I signal (Xue et al., 2021), the IGS reference products are based on an ionosphere-fee B1I/B3I combination and the corresponding antenna phase centers of the IGS antenna model (igs14_2188.atx).

While differences in the adopted antenna offsets for broadcast and precise ephemerides can be taken into account in a straightforward manner by

consideration of the corresponding PCO z-differences, further considerations are required for the handling of signal-specific group delays. Depending on the choice of a specific single- or dual-frequency user signal for the SISRE computations, different linear combinations of broadcast group delays or network-based DCB estimates must be applied to translate the respective satellite clock offsets to the selected signal. These corrections are summarized in Table 5 for the various signals of interest.

Considering only the global MEO satellites and neglecting correlations between radial orbit errors and clock offset errors, which play a subordinate role for BDS-3, the globally averaged signal-in-space range error can be expressed as:

$$\mathrm{SISRE} \approx \sqrt{R^2 + w^2(A^2 + C^2) + T^2} \tag{4}$$

Here, R, A, and C denote the root-mean square (RMS) orbit differences of broadcast and precise orbits and $w = 0.132$ is a weight factor representing the global average contribution of along-track and cross-track errors on the line-of-sight range (Montenbruck et al., 2018) at the altitude of the BDS-3 constellation. T represents the RMS clock offset differences, which are obtained after consideration of the respective antenna offsets and user-signal-specific group delay corrections, as well as subtraction of an epoch-wise constellation mean value representing the system time difference of broadcast and precise clock products. The orbit-only $\mathrm{SISRE}_{\mathrm{orb}}$ considering only R, A, and C is commonly used in SISRE analyses to separately quantify the contribution of orbit and clock errors. The total SISRE can then be expressed as the root-sum-square (RSS) of $\mathrm{SISRE}_{\mathrm{orb}}$ and the RMS clock errors T.

TABLE 5
Signal-Dependent Group Delay Corrections of Satellite Clock Offsets in Broadcast Ephemerides (bce) and Precise Reference Ephemerides (ref) for SISRE Monitoring of Selected Single- and Dual-Frequency Navigation Services

Message	User signal(s)	Broadcast	Reference
D1	B1I	$dt^{\mathrm{sat}}_{\mathrm{bce}} - \mathrm{TGD}_1$	$dt^{\mathrm{sat}}_{\mathrm{ref}} - \left(-\frac{f^2_{\mathrm{B3}}}{f^2_{\mathrm{B1\text{-}2}} - f^2_{\mathrm{B3}}}\mathrm{DCB}_{\mathrm{C2I\text{-}C6I}}\right)$
	B3I	$dt^{\mathrm{sat}}_{\mathrm{bce}}$	$dt^{\mathrm{sat}}_{\mathrm{ref}} - \left(-\frac{f^2_{\mathrm{B1\text{-}2}}}{f^2_{\mathrm{B1\text{-}2}} - f^2_{\mathrm{B3}}}\mathrm{DCB}_{\mathrm{C2I\text{-}C6I}}\right)$
	B1I, B3I	$dt^{\mathrm{sat}}_{\mathrm{bce}} - \left(\frac{f^2_{\mathrm{B1\text{-}2}}}{f^2_{\mathrm{B1\text{-}2}} - f^2_{\mathrm{B3}}}\mathrm{TGD}_1\right)$	$dt^{\mathrm{sat}}_{\mathrm{ref}}$
CNAV-1	B1C	$dt^{\mathrm{sat}}_{\mathrm{bce}} - \mathrm{TGD}_{\mathrm{B1Cp}}$	$dt^{\mathrm{sat}}_{\mathrm{ref}} - \left(\mathrm{DCB}_{\mathrm{C1P\text{-}C6I}} - \frac{f^2_{\mathrm{B2\text{-}1}}}{f^2_{\mathrm{B1\text{-}2}} - f^2_{\mathrm{B3}}}\mathrm{DCB}_{\mathrm{C2I\text{-}C6I}}\right)$
	B3I	$dt^{\mathrm{sat}}_{\mathrm{bce}}$	$dt^{\mathrm{sat}}_{\mathrm{ref}} - \left(-\frac{f^2_{\mathrm{B1\text{-}2}}}{f^2_{\mathrm{B1\text{-}2}} - f^2_{\mathrm{B3}}}\mathrm{DCB}_{\mathrm{C2I\text{-}C6I}}\right)$
	B1C, B3I	$dt^{\mathrm{sat}}_{\mathrm{bce}} - \left(\frac{f^2_{\mathrm{B1}}}{f^2_{\mathrm{B1}} - f^2_{\mathrm{B3}}}\mathrm{TGD}_{\mathrm{B1Cp}}\right)$	$dt^{\mathrm{sat}}_{\mathrm{ref}} - \left(+\frac{f^2_{\mathrm{B1}}}{f^2_{\mathrm{B1}} - f^2_{\mathrm{B3}}}\mathrm{DCB}_{\mathrm{C1P\text{-}C6I}} - \frac{f^2_{\mathrm{B1\text{-}2}}}{f^2_{\mathrm{B1\text{-}2}} - f^2_{\mathrm{B3}}}\mathrm{DCB}_{\mathrm{C2I\text{-}C6I}}\right)$
	B2a	$dt^{\mathrm{sat}}_{\mathrm{bce}} - \mathrm{TGD}_{\mathrm{B2ap}}$	$dt^{\mathrm{sat}}_{\mathrm{ref}} - \left(\mathrm{DCB}_{\mathrm{C5P\text{-}C6I}} - \frac{f^2_{\mathrm{B2\text{-}1}}}{f^2_{\mathrm{B1\text{-}2}} - f^2_{\mathrm{B3}}}\mathrm{DCB}_{\mathrm{C2I\text{-}C6I}}\right)$
	B1C, B2a	$dt^{\mathrm{sat}}_{\mathrm{bce}} - \left(\frac{f^2_{\mathrm{B1}}}{f^2_{\mathrm{B1}} - f^2_{\mathrm{B2a}}}\mathrm{TGD}_{\mathrm{B1Cp}} - \frac{f^2_{\mathrm{B2a}}}{f^2_{\mathrm{B1}} - f^2_{\mathrm{B2a}}}\mathrm{TGD}_{\mathrm{B2ap}}\right)$	$dt^{\mathrm{sat}}_{\mathrm{ref}} - \left(\frac{f^2_{\mathrm{B1}}}{f^2_{\mathrm{B1}} - f^2_{\mathrm{B2a}}}\mathrm{DCB}_{\mathrm{C1P\text{-}C6I}} - \frac{f^2_{\mathrm{B2a}}}{f^2_{\mathrm{B1}} - f^2_{\mathrm{B2a}}}\mathrm{DCB}_{\mathrm{C5P\text{-}C6I}} - \frac{f^2_{\mathrm{B1\text{-}2}}}{f^2_{\mathrm{B1\text{-}2}} - f^2_{\mathrm{B3}}}\mathrm{DCB}_{\mathrm{C2I\text{-}C6I}}\right)$

Note: f_b denotes the frequency for the frequency band b (cf. Table 1).

TABLE 6
SISRE Values and Contributions for BDS-3 MEO Satellites

Message	Signals	$SISRE_{orb}$	T	SISRE	T_0	T_b
D1	B1I	0.12	0.38	0.40	0.25	0.28
	B3I	0.12	0.44	0.45	0.25	0.35
	B1I, B3I	0.12	0.60	0.62	0.25	0.56
CNAV-1	B1C	0.11	0.42	0.43	0.25	0.33
	B3I	0.11	0.44	0.45	0.25	0.35
	B1C, B3I	0.11	0.53	0.54	0.25	0.48
	B2a	0.11	0.41	0.43	0.25	0.32
	B1C, B2a	0.11	0.45	0.46	0.25	0.38
D1+CNAV-2	B1I, B2a	0.11	0.42	0.43	0.25	0.34

Note: All values in m.

Based on the broadcast ephemerides for the legacy (D1; CSNO, 2019) and modernized (CNAV-1; CSNO, 2017a) navigation messages and the precise GFZ reference product along with CAS DCBs, SISRE values of the BDS-3 MEO constellation were evaluated for the various single- and dual-frequency user signals over a 30-day period in November 2021. The results collated in Table 6 illustrate the dominant contribution of the combined clock and group delay errors T to the overall SISRE, which ranges from 0.4 m to 0.6 m depending on the user signal adopted for the comparison of broadcast and precise products.

Similar to the comparison of broadcast and precise group delays (Figure 6), the comparison of group-delay corrected clock offsets exhibits the presence of notable satellite-specific mean values that made up a substantial fraction of the overall T error. Values of these clock offset biases $\Delta cdt_s^i = cdt_{\mathrm{bce},s}^i - cdt_{\mathrm{ref},s}^i$ for individual satellites i as estimated from the 1-month data arc are shown in Figure 9 for the various single-frequency user signals s.

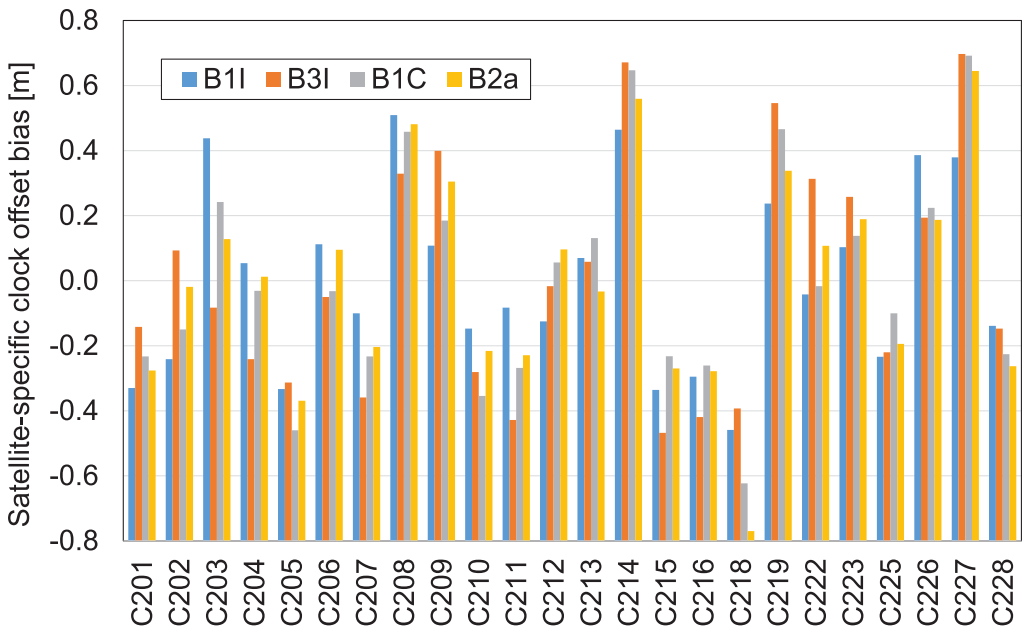

FIGURE 9 Satellite-specific clock biases Δcdt_s^i of broadcast ephemerides relative to precise ephemerides for different user signals s and satellites i

Overall, the satellite-specific systematic clock errors cover a range of roughly ±0.6 m, or, equivalently, ±2 ns and are highly correlated across the various signals. Their RMS values T_b over all satellites of the BDS-3 constellation are provided in Table 6 along with the RMS clock offset differences T_0 that remain after correcting the satellite-specific clock offset biases. T_0 represents random errors in the forecast of satellite clock offsets by the BeiDou ground segment and amounts to 0.25 m irrespective of the selected user signal. Considering only these contributions in addition to the orbit errors, signal-in-space range errors of 0.28 cm might be achieved in BDS-3. In practice, however, the overall SISRE budget is seriously degraded by the presence of systematic biases in the group-delay-corrected clock offsets.

From Figure 9, a notable correlation of these satellite-specific biases for different user signals may be observed. Differences between individual curves match the corresponding TGD-DCB differences discussed in the previous section and are typically smaller than the satellite-specific biases in the B3I clock offsets provided in the broadcast ephemerides. In particular, a good consistency is observed for the Δcdt^i_{B1I}, Δcdt^i_{B1C}, and Δcdt^i_{B2a} clock offset errors, which reflects the good consistency of the respective broadcast and CAS group delay values.

The Δcdt^i_{B3I} clock offset bias exhibits the largest RMS value among the four signals and shows a partial correlation with the $\Delta cdt^i_{B1I} - \Delta cdt^i_{B3I}$ difference or equivalently the $TGD_1 - DCB_{C2I\text{-}C6I}$. This correlation is also evidenced by the fact that the T_b error for dual-frequency B1I/B3I user signals is smaller (see Table 6) than would be expected for the propagation of statistically independent B1I and B3I contributions in the ionosphere-free linear combination.

Overall, the SISRE analysis shows that next to satellite-specific group delay differences between broadcast ephemerides and precise IGS products, similar inconsistencies apply as well for the broadcast clock offsets. Following Yang et al. (2021), broadcast clock offsets for BeiDou satellites are derived from observations of dedicated two-way satellite time comparison (TSTC) stations. While it remains unclear which calibration techniques are used to translate these TSTC observations into B3I-specific clock offsets for users of the L-band GNSS ranging signals, incompatibilities of the employed calibrations with common user receivers are obvious from the SISRE analysis. Similar to the update of broadcast group delay estimation processes performed in 2017 (Zhang et al., 2020a), determination of the B3I clock offsets in the BeiDou ground segment may therefore need to be revisited to further improve the consistency of BeiDou broadcast ephemerides with current GNSS user equipment.

Even though broadcast ephemeris users cannot presently overcome the problem of satellite-specific clock offset biases in the navigation message in pseudorange-based positioning and timing applications, Table 6 shows that some flexibility exists to minimize the combined impact of broadcast clock and group delay errors. In fact, the partial correlation of the satellite-specific B3I clock offset biases and the satellite-specific TGD_1 errors results in a lower SISRE for B1I users than for B3I users. Likewise, B1C and B2a SISRE values are smaller than those for the B3I signal. For dual-frequency users, use of the ionosphere-free B1C/B2a combination results in a SISRE of 46 cm, which clearly outperforms the legacy B1I/B3I signal combination with its SISRE of 62 cm. An even smaller SISRE of 43 cm can be obtained when working with a B1I/B2a dual-frequency combination and making joint use of the corresponding TGD_1 and TGD_{B2ap} group delays from the D1 and CNAV-2 navigation messages. This should not, however, be mistaken as an indicator for a superior quality of the legacy B1I signal compared to the new B1C signal, but rather reflects the partial compensation of the systematic B3I clock offset biases by corresponding satellite-specific biases in the TGD_1 group delays.

8 | SUMMARY AND CONCLUSIONS

Group delays of BDS-2 and BDS-3 satellites exhibit a high temporal stability except in limited periods of on-ground or onboard equipment reconfigurations. Using global monitoring networks, differential code biases can be determined as part of ionospheric analyses or by using pre-computed ionosphere maps. Both methods provide a representative precision of 0.1 ns, which describes the day-to-day repeatability of DCB estimates and includes both estimation uncertainties as well as physical bias changes. However, the high precision contrasts with a much lower accuracy as evidenced by the comparison of different DCB products. Inconsistencies between different group delay determinations are attributed to chip shape distortions in BeiDou-2 and BeiDou-3 ranging signals which inhibit an unambiguous partitioning of the overall biases in the entire signal chain into distinct satellite and receiver contributions. As a result, an obvious dependence of satellite group delay estimates on the type and architecture of the employed receivers could be observed. This affects both the consistency of DCB products based on public geodetic receiver networks as well as the compatibility of broadcast group delays with common BDS receivers.

The most pronounced impact can be observed for the legacy B1I signal at the 1561.098-MHz sideband of the L1/E1/B1 frequency. For BeiDou-3 differential code biases involving this signal, satellite-specific inconsistencies of up to ±2 ns (1 ns RMS) can be observed between broadcast timing group delays and public DCB products. Comparing TGD_1 values for the B1I-B3I group delay from broadcast navigation messages with $DCB_{C2I\text{-}C6I}$ estimates from IGS monitoring stations, a systematic offset can be identified between satellites of the regional BDS-2 constellation and the new global BDS-3 system. Closer inspection shows a pronounced dependency of this offset on the employed receiver type.

Considering four brand-specific subsets of the IGS networks, BDS-3 vs. BDS-2 offsets in the $TGD_1 - DCB_{C2I\text{-}C6I}$ difference ranging from 1.5 to 5 ns were identified. As a consequence, a receiver-specific inter-system bias between BDS-2 and BDS-3 would need to be considered for mixed processing of the regional and global BeiDou system. This is particularly relevant for pseudorange-based positioning and timing applications using broadcast navigation messages, but also applies to some extent for precise positioning applications (e.g., when aiming at a fully consistent treatment of pseudoranges for ambiguity resolution).

Considering the global constellation of BDS-3 MEO satellites, satellite group delays for the new B1C and B2a signals exhibit a notably better (0.5 ns) consistency of broadcast TGDs and IGS DCB products as well as a reduced dependency on the receiver types compared to the B1I signal. This applies both for B1C and B2a group delays relative to the B3I signal that serves as reference for BeiDou broadcast clock offsets, but even more for the differential code delays between B1C and B2a signals. Here, consistency at the level of about 0.3 to 0.4 ns was achieved among different DCB solutions and in comparison with broadcast TGDs.

Incompatibilities of broadcast values with common geodetic receivers are not limited to differential code biases but also apply to satellite clock offset parameters. In contrast to all other navigation systems, BeiDou system time (BDT) refers to a single-frequency (B3I) signal, which inhibits direct access to BDT using an ionosphere-free linear combination of dual-frequency pseudorange observations. Thus, satellite-specific errors in broadcast clock offsets and broadcast group delays jointly affect the achievable positioning and timing accuracy with standalone BeiDou receivers. Considering the contribution of clock and bias errors to the

signal-in-space range error (SISRE), notable differences may be observed for the variety of signals transmitted by the global BDS-3 constellation.

When comparing broadcast ephemerides with precise orbit, clock, and bias products from the International GNSS Service, RMS SISRE values of about 40 cm to 45 cm were obtained for single-frequency users. The overall SISRE constitutes the root-sum-square of three contributions, namely orbit-only range errors of 11 cm to 12 cm RMS, random clock offset errors of about 25 cm RMS, and systematic satellite-specific clock and bias errors of varying magnitude. The latter depends on the particular signal choice and exhibits an RMS scatter between 28 cm (for B1I, B1C, and B2a) and 35 cm for B3I across the constellation. Essentially, these errors reflect the inconsistent perception of chip shape distortions in the transmitted signals by common geodetic receivers compared to monitoring systems for broadcast clock and group delay determination in the BDS control segment.

As may be recognized, these signal- and satellite-specific errors already dominate the overall SISRE budget for single-frequency users but are even more pronounced for dual-frequency navigation. Here, satellite-specific RMS clock offset biases between about 34 cm for B1I/B2a users and 56 cm for B1I/B3I users are encountered. Even though the amplification of single-frequency errors is less pronounced than would be expected for the ionosphere-free combination of uncorrelated random errors, it results in a notable increase of the total RMS SISRE to roughly 43 cm to 62 cm. Systematic satellite- and receiver-dependent clock and group delay errors thus constitute the dominating contribution to the BDS-3 SISRE and the overall navigation accuracy.

Obviously, changes to the transmitted chip shapes would be difficult, if not impossible, to accomplish in the existing BeiDou constellation and can at best be expected for the next generation of satellites. As an alternative, ground-based solutions are required to better match the broadcast data with actual user equipment. By way of example, a notable improvement has earlier been achieved for BeiDou-2 legacy signals by changing from narrow to wide correlator spacing in the monitoring receivers for timing group delay determination. However, prospects for further adaptation of the clock offset and group delay determination in the BeiDou control segment to improve consistency with the average receiver are probably limited in view of the wide diversity of current receivers for mass-market and precise applications. For high precision timing receivers that are most notably affected by the observed inconsistencies, use of a standardized correlator architecture and spacing appears to be a feasible solution to facilitate access to BeiDou system time and to enable consistent time chain calibrations. As a general measure, transition to modernized BeiDou signals is encouraged. While this excludes joint use of BDS-3 along with satellites from the regional BDS-2 system, it would pay off in terms of better single point positioning and timing accuracy for standalone BeiDou users around the globe.

Aside from benefits in terms of multipath suppression and weak signal tracking offered by the advanced signal modulation, use of the B1C/B2a signals instead of B1I/B3I appears most beneficial. It would greatly improve the compatibility of broadcast information with current receivers and reduce the overall SISRE budget for pseudorange-based single point dual-frequency navigation by more than 25%. Furthermore, use of these signals would contribute to a better consistency of satellite group delays and clock offsets estimated from heterogeneous receiver networks.

Along with this recommendation, a transition of the clock reference signal from B1I/B3I to B1C/B2a is encouraged for the generation of precise BDS-3 ephemeris products. With more than 80 receivers supporting the tracking of new signals in

the IGS network by the end of 2021, transition to B1C and B2a clock products appears well within reach and could help to further increase the contribution of BDS-3 for PPP and timing applications. Aside from an improved consistency of broadcast and precise ephemeris products for BDS-3, use of modernized signals is also desirable for multi-GNSS processing. In particular, a joint Galileo and BDS-3 processing would benefit from a harmonized signal set with similar signal structures and common frequency bands, which helps to minimize signal-related biases between the two constellations.

ACKNOWLEDGMENTS

The authors acknowledge the contributions of all station operators, data centers, and analysis centers of the International GNSS Service. NW author acknowledges the financial support from the National Key R&D Program of China (2021YFB3901301).

REFERENCES

Banville, S. (2021). *Upcoming convention regarding PCO and biases* (IGS Mail No. 8113). https://lists.igs.org/pipermail/igsmail/2021/008109.html

Beer, S., Wanninger, L., & Heßelbarth, A. (2021). Estimation of absolute GNSS satellite antenna group delay variations based on those of absolute receiver antenna group delays. *GPS Solutions*, *25*(3), 110. https://doi.org/10.1007/s10291-021-01137-8

Betz, J. W. (2016). *Engineering satellite-based navigation and timing: Global navigation satellite systems, signals, and receivers*. Wiley-IEEE Press.

Cai, H., Chen, G., Jiao, W., Chen, K., Xu, T., & Wang, H. (2016). An initial analysis and assessment on final products of iGMAS. In J. Sun, J. Liu, S. Fan, & F. Wang (Eds.) *China Satellite Navigation Conference (CSNC) 2016 Proceedings: Volume III* (pp. 515–527). https://doi.org/10.1007/978-981-10-0940-2_45

China Satellite Navigation Office (CSNO). (2016). *BeiDou navigation satellite system signal in space interface control document: Open service signal* (Version 2.1). China Satellite Navigation Office. https://en.beidou.gov.cn/SYSTEMS/ICD/201806/P020180608523308843290.pdf

China Satellite Navigation Office (CSNO). (2017a). *BeiDou navigation satellite system signal in space interface control document: Open service signal B1C* (Version 1.0). China Satellite Navigation Office. http://www.beidou.gov.cn/xt/gfxz/201712/P020171226741342013031.pdf

China Satellite Navigation Office (CSNO). (2017b). *BeiDou navigation satellite system signal in space interface control document: Open service signal B2a* (Version 1.0). China Satellite Navigation Office. http://www.beidou.gov.cn/xt/gfxz/201712/P020171226742357364174.pdf

China Satellite Navigation Office (CSNO). (2018). *BeiDou navigation satellite system signal in space interface control document: Open service signal B3I* (Version 1.0). China Satellite Navigation Office. http://www.beidou.gov.cn/xt/gfxz/201802/P020180209623601401189.pdf

China Satellite Navigation Office (CSNO). (2019). *BeiDou navigation satellite system signal in space interface control document: Open service signal B1I* (Version 3.0). China Satellite Navigation Office. http://www.beidou.gov.cn/xt/gfxz/201902/P020190227593621142475.pdf

China Satellite Navigation Office (CSNO). (2020). *BeiDou navigation satellite system signal in space interface control document: Open service signal B2b* (Version 1.0). China Satellite Navigation Office. http://en.beidou.gov.cn/SYSTEMS/ICD/202008/P020200803539206360377.pdf

China Satellite Navigation Office Test and Assessment Research Center (CSNO-TARC). (2022). *Satellite parameters*. Test and Assessment Research Center of China Satellite Navigation Office. http://www.csno-tarc.cn/en/datacenter/satelliteparameters

Deng, Z., Nischan, T., & Bradke, M. (2017). *Multi-GNSS rapid orbit-, clock- & EOP-product series*. GFZ Data Services. https://doi.org/10.5880/GFZ.1.1.2017.002

Esenbuga, Ö. G., Hauschild, A., & Steigenberger, P. (2020). Impact of GPS flex power on differential code bias estimation for Block IIR-M and IIF satellites. *Proc. of the 33rd International Technical Meeting of the Satellite Division of the Institute of Navigation (ION GNSS+ 2020)*, 2922–2930. https://doi.org/10.33012/2020.17634

Gong, X., Lou, Y., Zheng, F., Gu, S., Shi, C., Liu, J., & Jing, G. (2018). Evaluation and calibration of BeiDou receiver-related pseudorange biases. *GPS Solutions*, *22*(4), 98. https://doi.org/10.1007/s10291-018-0765-3

Gu, S., Wang, Y., Zhao, Q., Zheng, F., & Gong, X. (2020). BDS-3 differential code bias estimation with undifferenced uncombined model based on triple-frequency observation. *Journal of Geodesy*, *94*(4), 45. https://doi.org/10.1007/s00190-020-01364-w

Guo, F., Zhang, X., & Wang, J. (2015). Timing group delay and differential code bias corrections for BeiDou positioning. *Journal of Geodesy*, *89*(5), 427–445. https://doi.org/10.1007/s00190-015-0788-2

Hauschild, A. (2017). Basic observation equations. In P. Teunissen & O. Montenbruck (Eds.) *Springer handbook of global navigation satellite systems* (pp. 561–582). Springer. https://doi.org/10.1007/978-3-319-42928-1_19

Hauschild, A., & Montenbruck, O. (2016). The effect of correlator and front-end design on GNSS pseudorange biases for geodetic receivers. *NAVIGATION*, *63*(4), 443–453. https://doi.org/10.1002/navi.165

He, C., Lu, X., Guo, J., Su, C., Wang, W., & Wang, M. (2020). Initial analysis for characterizing and mitigating the pseudorange biases of BeiDou navigation satellite system. *Satellite Navigation*, *1*(1), 3. https://doi.org/10.1186/s43020-019-0003-3

Hong, J., Tu, R., Zhang, R., Fan, L., Zhang, P., Han, J., & Lu, X. (2020). Analyzing the satellite-induced code bias variation characteristics for the BDS-3 via a 40 m dish antenna. *Sensors*, *20*(5). https://doi.org/10.3390/s20051339

Hwang, P. Y., McGraw, G. A., & Bader, J. R. (1999). Enhanced differential GPS carrier-smoothed code processing using dual-frequency measurements. *NAVIGATION*, *46*(2), 127–137. https://doi.org/10.1002/j.2161-4296.1999.tb02401.x

Johnston, G., Riddell, A., & Hausler, G. (2017). The International GNSS Service. In P. G. Teunissen & O. Montenbruck (Eds.) *Springer handbook of global navigation satellite systems* (pp. 967–982). Springer. https://doi.org/10.1007/978-3-319-42928-1_33

Langley, R. B., Teunissen, P. J. G., & Montenbruck, O. (2017). Introduction to GNSS. In P. Teunissen & O. Montenbruck (Eds.) *Springer handbook of global navigation satellite systems* (pp. 3–23). Springer. https://doi.org/10.1007/978-3-319-42928-1_1

Li, G., Zhang, D., Lin, Y., & Wang, J. (2021a). A closed-loop calibration method of the BeiDou time receiver. In C. Yang & J. Xie (Eds.) *China satellite navigation conference (CSNC) 2021 proceedings: Volume III* (pp. 74–85). https://doi.org/10.1007/978-981-16-3146-7_8

Li, M., & Yuan, Y. (2021). Estimation and analysis of BDS2 and BDS3 differential code biases and global ionospheric maps using BDS observations. *Remote Sensing*, *13*(3), 370. https://doi.org/10.3390/rs13030370

Li, R., Wang, N., Li, Z., Zhang, Y., Wang, Z., & Ma, H. (2021b). Precise orbit determination of BDS-3 satellites using B1C and B2a dual-frequency measurements. *GPS Solutions*, *25*(3), 95. https://doi.org/10.1007/s10291-021-01126-x

Li, X., Li, X., Liu, G., Xie, W., Guo, F., Yuan, Y., Zhang, K., & Feng, G. (2020). The phase and code biases of Galileo and BDS-3 BOC signals: Effect on ambiguity resolution and precise positioning. *Journal of Geodesy*, *94*(1), 9. https://doi.org/10.1007/s00190-019-01336-9

Li, X., Xie, W., Huang, J., Ma, T., Zhang, X., & Yuan, Y. (2019). Estimation and analysis of differential code biases for BDS3/BDS2 using iGMAS and MGEX observations. *Journal of Geodesy*, *93*(3), 419–435. https://doi.org/10.1007/s00190-018-1170-y

Lou, Y., Gong, X., Gu, S., Zheng, F., & Feng, Y. (2017). Assessment of code bias variations of BDS triple-frequency signals and their impacts on ambiguity resolution for long baselines. *GPS Solutions*, *21*(1), 177–186. https://doi.org/10.1007/s10291-016-0514-4

Lu, M., Li, W., Yao, Z., & Cui, X. (2019). Overview of BDS III new signals. *NAVIGATION*, *66*(1), 19–35. https://doi.org/10.1002/navi.296

Lu, M., & Yao, Z. (2020). BeiDou navigation satellite system. In Y. T. J. Morton, F. van Diggelen, J. J. Spilker Jr., B. W. Parkinson, S. Lo, & G. Gao (Eds.) *Position, navigation, and timing technologies in the 21st century: Integrated satellite navigation, sensor systems, and civil applications* (Vol. 1, pp. 143–170). Wiley. https://doi.org/10.1002/9781119458449.ch6

Montenbruck, O., Hauschild, A., & Steigenberger, P. (2014). Differential code bias estimation using multi-GNSS observations and global ionosphere maps. *NAVIGATION*, *61*(3), 191–201. https://doi.org/10.1002/navi.64

Montenbruck, O., & Steigenberger, P. (2022). *BRD400DLR: DLR's merged multi-GNSS broadcast ephemeris product in RINEX 4.00 format* [Data set]. DLR/GSOC. https://doi.org/10.57677/BRD400DLR

Montenbruck, O., Steigenberger, P., & Hauschild, A. (2018). Multi-GNSS signal-in-space range error assessment—methodology and results. *Advances in Space Research*, *61*(12), 3020–3038. https://doi.org/10.1016/j.asr.2018.03.041

Montenbruck, O., Steigenberger, P., & Hauschild, A. (2020). Comparing the 'Big 4'—a user's view on GNSS performance. *2020 IEEE/ION Position, Location and Navigation Symposium (PLANS)*, Portland, OR. https://doi.org/10.1109/PLANS46316.2020.9110208

Montenbruck, O., Steigenberger, P., Prange, L., Deng, Z., Zhao, Q., Perosanz, F., Romero, I., Noll, C., Sturze, A., Weber, G., Schmid, R., MacLeod, K., & Schaer, S. (2017). The multi-GNSS experiment (MGEX) of the International GNSS Service (IGS)—achievements, prospects and challenges. *Advances in Space Research*, *59*(7), 1671–1697. https://doi.org/10.1016/j.asr.2017.01.011

Rebischung, P., & Schmid, R. (2016). IGS14/igs14.atx: a new framework for the IGS products. *AGU Fall Meeting*, San Francisco, CA. https://www.researchgate.net/publication/311654495_IGS14igs14atx_a_new_framework_for_the_IGS_products

Romero, I. (2021). *RINEX: The receiver independent exchange format* (Version 4.00). IGS. https://files.igs.org/pub/data/format/rinex_4.00.pdf

Schaer, S. (2016). *SINEX_BIAS—Solution (software/technique) independent exchange format for GNSS biases* (Version 1.0). AIUB. https://files.igs.org/pub/data/format/sinex_bias_100.pdf

Sleewaegen, J.-M., & Clemente, F. (2018). Quantifying the pilot-data bias on all current GNSS signals and satellites. *Proc. of the IGS Workshop 2018*. https://s3-ap-southeast-2.amazonaws.com/igs-acc-web/igs-acc-website/workshop2018/presentations/IGSWS-2018-PY05-05.pdf

Wang, N., Li, Z., Montenbruck, O., & Tang, C. (2019). Quality assessment of GPS, Galileo and BeiDou-2/3 satellite broadcast group delays. *Advances in Space Research*, *64*(9), 1764–1779. https://doi.org/10.1016/j.asr.2019.07.029

Wang, N., Yuan, Y., Li, Z., Montenbruck, O., & Tan, B. (2016). Determination of differential code biases with multi-GNSS observations. *Journal of Geodesy*, *90*(3), 209–228. https://doi.org/10.1007/s00190-015-0867-4

Wang, Q., Jin, S., Yuan, L., Hu, Y., Chen, J., & Guo, J. (2020). Estimation and analysis of BDS-3 differential code biases from MGEX observations. *Remote Sensing*, *12*(1). https://doi.org/10.3390/rs12010068

Wanninger, L., & Beer, S. (2015). BeiDou satellite-induced code pseudorange variations: Diagnosis and therapy. *GPS Solutions*, *19*(4), 639–648. https://doi.org/10.1007/s10291-014-0423-3

Wilson, B., & Mannucci, A. (1994). Extracting ionospheric measurements from GPS in the presence of anti-spoofing. *Proc. of the 7th International Technical Meeting of the Satellite Division of the Institute of Navigation (ION GPS 1994)*, Salt Lake City, UT, 1599–1608. https://www.ion.org/publications/abstract.cfm?articleID=3982

Xing, N. (2011). Hardware delay solution of regional satellite navigation system. *Geomatics and Information Science of Wuhan University*, *36*(10), 1218–1221. https://www.semanticscholar.org/paper/Hardware-Delay-Solution-of-Regional-Satellite-Nan/48c640afb9b8af760ad5230df441969489f531c8

Xue, B., Wang, H., & Yuan, Y. (2021). Performance of BeiDou-3 signal-in-space ranging errors: Accuracy and distribution. *GPS Solutions*, *25*(1). https://doi.org/10.1007/s10291-020-01057-z

Yang, Y., Gao, W., Guo, S., Mao, Y., & Yang, Y. (2019). Introduction to BeiDou-3 navigation satellite system. *NAVIGATION*, *66*(1), 7–18. https://doi.org/10.1002/navi.291

Yang, Y., Yang, Y., Hu, X., Tang, C., Guo, R., Zhou, Z., Xu, J., Pan, J., & Su, M. (2021). BeiDou-3 broadcast clock estimation by integration of observations of regional tracking stations and inter-satellite links. *GPS Solutions*, *25*(2), 57. https://doi.org/10.1007/s10291-020-01067-x

Yao, Z., Guo, F., Ma, J., & Lu, M. (2017). Orthogonality-based generalized multicarrier constant envelope multiplexing for DSSS signals. *IEEE Transactions on Aerospace and Electronic Systems*, *53*(4), 1685–1698. https://doi.org/10.1109/TAES.2017.2671580

Yao, Z., Zhang, J., & Lu, M. (2016). ACE-BOC: Dual-frequency constant envelope multiplexing for satellite navigation. *IEEE Transactions on Aerospace and Electronic Systems*, *52*(1), 466–485. https://doi.org/10.1109/TAES.2015.140607

Yinger, C. H., Feess, W. A., Di Esposti, R., Chasko, A., Cosentino, B., Wilson, B., & Wheaton, B. (1999). GPS satellite interfrequency biases. *Proc. of the 55th Annual Meeting of the Institute of Navigation,* Cambridge, MA, 347–354. https://www.ion.org/publications/abstract.cfm?articleID=1329

Zhang, Y., Chen, J., Gong, X., & Chen, Q. (2020a). The update of BDS-2 TGD and its impact on positioning. *Advances in Space Research*, *65*(11), 2645–2661. https://doi.org/10.1016/j.asr.2020.03.011

Zhang, Y., Kubo, N., Chen, J., Chu, F.-Y., Wang, A., & Wang, J. (2020b). Apparent clock and TGD biases between BDS-2 and BDS-3. *GPS Solutions*, *24*(1), 27. https://doi.org/10.1007/s10291-019-0933-0

Zhang, Y., Wang, H., Chen, J., Wang, A., Meng, L., & Wang, E. (2020c). Calibration and impact of BeiDou satellite-dependent timing group delay bias. *Remote Sensing*, *12*(1). https://doi.org/10.3390/rs12010192

Zhu, Y., Tan, S., Feng, L., Cui, X., Zhang, Q., & Jia, X. (2020). Estimation of the DCB for the BDS-3 new signals based on BDGIM constraints. *Advances in Space Research*, *66*(6), 1405–1414. https://doi.org/10.1016/j.asr.2020.05.019

How to cite this article: Montenbruck, O., Steigenberger, P., Wang, N., & Hauschild, A. (2022) Characterization and performance assessment of BeiDou-2 and BeiDou-3 satellite group delays. *NAVIGATION, 69*(3). https://doi.org/10.33012/navi.526